

Quantitative Susceptibility MRI to Detect Brain Iron in Amyotrophic Lateral Sclerosis

Julio Acosta-Cabronero, PhD • Judith Machts, PhD • Stefanie Schreiber, MD • Susanne Abdulla, MD • Katja Kollwe, MD • Susanne Petri, MD • Nicola Spotorno, PhD • Joern Kaufmann, PhD • Hans-Jochen Heinze, MD • Reinhard Dengler, MD • Stefan Vielhaber, MD • Peter J. Nestor, PhD, FRACP

From the German Center for Neurodegenerative Diseases, Magdeburg, Germany (J.A., J.M., N.S., H.J.H., P.J.N.); Wellcome Centre for Human Neuroimaging, UCL Institute of Neurology, University College London, 12 Queen Square, London WC1N 3BG, England (J.A.); Department of Neurology, Otto von Guericke University, Magdeburg, Germany (J.M., S.S., S.A., J.K., H.J.H., S.V.); Department of Neurology and Clinical Neurophysiology, Hannover Medical School, Hannover, Germany (S.A., K.K., S.P., R.D.); Leibniz Institute for Neurobiology, Magdeburg, Germany (H.J.H.); and Queensland Brain Institute, University of Queensland, Brisbane, Australia (P.J.N.). Received January 15, 2018; revision requested March 13; final revision received May 9; accepted May 17. **Address correspondence to** J.A. (e-mail: jac@cantab.net).

Supported by the German Center for Neurodegenerative Diseases Helmholtz Association. The Wellcome Centre for Human Neuroimaging is supported by core funding from Wellcome (203147/Z/16/Z).

Conflicts of interest are listed at the end of this article.

Radiology 2018; ■:1–9 • <https://doi.org/10.1148/radiol.2018180112> • Content codes:  

Purpose: To investigate the whole-brain landscape of iron-related abnormalities in amyotrophic lateral sclerosis (ALS) by using the in vivo MRI technique of quantitative susceptibility mapping (QSM).

Materials and Methods: For this prospective study, 28 patients with ALS (mean age, 61 years; age range, 43–77 years; 18 men [mean age, 61 years; range, 43–77 years] and 10 women [mean age, 61 years; range, 47–74 years]) recruited between January 17, 2014, and September 4, 2015, and 39 matched control subjects (mean age, 61 years; age range, 39–77 years; 24 men [mean age, 62 years; range, 39–77 years] and 15 women [mean age, 59 years; range, 39–73 years]) were examined by using structural and susceptibility 3.0-T MRI techniques. Group data were cross sectionally compared with family-wise error (FWE) corrections by using voxel-based morphometry (random-field theory), cortical thickness analysis (Monte Carlo simulated), subcortical volumetry (Bonferroni-corrected Wilcoxon rank-sum testing), and QSM analysis (cluster-enhanced whole-brain permutation testing and Bonferroni-corrected rank-sum testing in regions of interest). In patients with ALS, a potential relationship between diffusion and susceptibility measurements in the corticospinal tracts (CSTs) was also examined by using Spearman rank-correlation tests.

Results: Conventional structural measures failed to identify atrophy in the present cohort (FWE $P > .05$). However, QSM identified several whole-brain abnormalities (FWE $P < .05$) in ALS. Regionally, higher susceptibility (expressed as means in parts per million \pm standard errors of the mean) was confirmed in the motor cortex (ALS = 0.0188 ± 0.0003 , control = 0.0173 ± 0.0003 ; $P < .001$), the left substantia nigra (ALS = 0.127 ± 0.004 , control = 0.113 ± 0.003 ; $P = .008$), the right substantia nigra (ALS = 0.141 ± 0.005 , control = 0.120 ± 0.003 ; $P < .001$), the globus pallidus (ALS = 0.086 ± 0.003 , control = 0.075 ± 0.002 ; $P = .003$), and the red nucleus (ALS = 0.115 ± 0.004 , control = 0.098 ± 0.003 ; $P < .001$). Lower susceptibility was found in CST white matter (ALS = -0.047 ± 0.001 , control = -0.043 ± 0.001 ; $P = .01$). Nigral and pallidal QSM values were cross correlated in ALS ($\rho^2 = 0.42$, $P < .001$), a phenomenon visually traceable in many individual patients. QSM in the CST in ALS also correlated with diffusion-tensor metrics in this tract ($\rho^2 = 0.25$, $P = .007$).

Conclusion: Whole-brain MRI quantitative susceptibility mapping analysis is sensitive to tissue alterations in amyotrophic lateral sclerosis that may be relevant to pathologic changes.

©RSNA, 2018

Amyotrophic lateral sclerosis (ALS) is a devastating neurodegenerative disease characterized by progressive damage to the motor system leading to irreversible paralysis of spinal and bulbar muscles, often accompanied or followed by cognitive dysfunction, with some clinical ALS presentations also meeting criteria for frontotemporal dementia (FTD) (1). The histopathologic hallmark of ALS—phosphorylated 43kDa TAR DNA-binding protein (pTDP-43) (2)—appears to involve primarily the motor nuclei of cranial nerves V, VII, and X–XII, the primary motor cortex, and the spinal cord. Early pathologic burden has also been identified in the reticular formation, red nucleus, and prefrontal cortex, as well as in the prefrontal, postcentral and striatal regions, with advanced disease also often involving temporal lobe regions, including the hippocampus (3).

The topographic distribution of pTDP-43 inclusions may, however, not necessarily be the only explanation for neurodegeneration; a further potentially relevant process is the mismanagement of metals such as iron or copper (4). Recent work in mouse models has demonstrated that iron chelation can decrease pathologic protein aggregation, enhance antiapoptotic protein expression, delay disease onset, prevent motor neuron loss, and, overall, extend the rodents' lifespans (5,6), reinforcing the view that brain iron might have an important role in ALS pathogenesis.

MRI is potentially ideal for monitoring metal levels in vivo because of the impact that iron species have on magnetic susceptibility, a fundamental physical property that can be approximated by using a recently validated technique, quantitative susceptibility mapping (QSM) (7). QSM has shown potential to detect

Abbreviations

ALS = amyotrophic lateral sclerosis, ALSFRS-R = ALS Functional Rating Scale Revised, CST = corticospinal tract, DTI = diffusion-tensor imaging, ECAS = Edinburgh Cognitive and Behavioral ALS Screen, FTD = frontotemporal dementia, FWE = family-wise error, GP = globus pallidus, MoCA = Montreal Cognitive Assessment, pTDP-43 = phosphorylated 43kDa TAR DNA-binding protein, QSM = quantitative susceptibility mapping, ROI = region of interest, SN = substantia nigra

Summary

Quantitative susceptibility mapping alterations in amyotrophic lateral sclerosis involve the motor cortex, corticospinal tracts, and a range of subcortical nuclei. This distribution is consistent with the known pattern of brain degeneration in this disease.

Implications for Patient Care

- There is a distinct pattern of iron deposition in amyotrophic lateral sclerosis (ALS) that can be identified by using quantitative susceptibility mapping MRI.
- Susceptibility measurements in ALS were abnormal in the motor cortex, corticospinal tracts, and a range of subcortical nuclei.
- Abnormalities consistent with iron deposition are present in areas of the brain that have been previously associated with neurodegeneration in ALS.

iron-related motor cortex alterations in ALS and other motor neuron disorders (8). However, the global distribution of abnormal QSM levels in ALS and its significance relative to standard structural MRI markers has not yet been elucidated. We hypothesized that whole-brain QSM would capture a distribution of perturbations in iron concentration preferentially affecting the central nervous system structures relevant to the motor system in this disease.

Materials and Methods

Study Participants

The local ethics committee approved our prospective study (140/14), with all subjects giving written informed consent prior to their inclusion. A cohort of patients with ALS (mean age, 61 years; age range, 43–77 years; 18 men [mean age, 61 years; range, 43–77 years] and 10 women [mean age, 61 years; range, 47–74 years]) recruited between January 17, 2014, and September 4, 2015 (by S.V., an ALS specialist with 25 years of experience), were grouped into disease phenotypes according to recently specified criteria based on results of clinical examination (9) and electromyography (10). At the time of MRI assessment, 28 patients displayed a variable combination of upper motor neuron signs (spasticity, clonus, pathologically brisk reflexes, pyramidal signs) and lower motor neuron signs (wasting, weakness, fasciculations) in the upper and lower limbs, in turn fulfilling the El Escorial criteria for definite or probable ALS (11). As summarized in Figure 1, patients with bulbar phenotype or pure upper motor neuron disease variants (also comprising primary lateral sclerosis and pure lower motor neuron disease variants including flail arm, flail limb, and progressive muscular atrophy) were excluded, as were those with concomitant FTD; the latter was defined on clinical grounds (including caregiver reports) in accordance with proposed di-

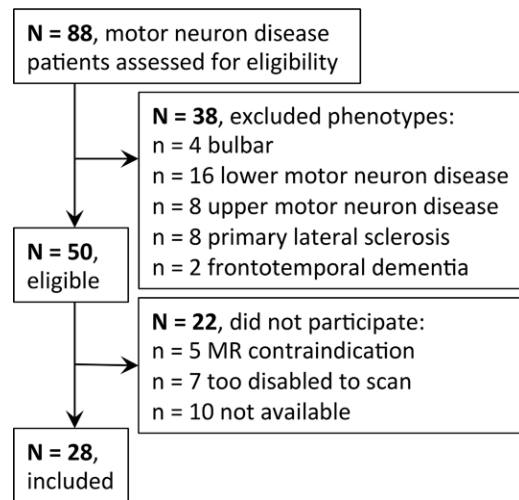


Figure 1: Summary of patient recruitment and exclusions.

agnostic criteria (12). Furthermore, there were no patients with primary progressive aphasia. Patients' functional and general cognitive status was assessed by using the ALS Functional Rating Scale Revised (ALSFRS-R) and the Edinburgh Cognitive and Behavioral ALS Screen (ECAS) and Montreal Cognitive Assessment (MoCA), respectively. Genetic testing for identification of *C9orf72* (chromosome 9 open reading frame 72) expansion carriers and *SOD1* (superoxide dismutase 1) mutation carriers was performed in 20 (71%) patients and identified two patients (approximately 10%) with the *C9orf72* gene expansion. Thirty-nine healthy control subjects were carefully selected for imaging comparisons by individual age and sex matching (mean age, 61 years; age range, 39–77 years; 24 men [mean age, 62 years; range, 39–77 years] and 15 women [mean age, 59 years; range, 39–73 years]). All control subjects were free of neurologic illness and performed normally on cognitive screening tests (Mini-Mental State Examination score \geq 28). All demographic details are summarized in the Table.

Imaging Protocol

MRI measurements were performed on a Siemens Verio 3.0-T system with a 32-channel head coil for reception (Siemens Medical Systems, Erlangen, Germany). Susceptibility MRI was performed with a three-dimensional, fully flow-compensated, spoiled gradient-echo pulse sequence with the following parameters: flip angle, 17°; echo time msec/repetition time msec, 20/28; and receiver bandwidth, 100 Hz/pixel. Reconstruction matrix dimensions were 256 \times 224 \times 80, with a voxel resolution of 1 \times 1 \times 2 mm³. Parallel imaging was enabled, with two-fold acceleration yielding an imaging time of 5 minutes 32 seconds.

T1-weighted magnetization-prepared rapid gradient-echo anatomic images were also acquired with the following parameters: inversion time, 1100 msec; flip angle, 7°; 4.82/2500; and bandwidth = 140 Hz/pixel. Matrix dimensions were 256 \times 256 \times 192 (7/8 phase partial Fourier), with a voxel size of 1 \times 1 \times 1 mm³. Parallel imaging was also enabled with two-fold acceleration.

Table 1: Study Demographic Details

Characteristic	Control Subjects (<i>n</i> = 39)	Patients with ALS (<i>n</i> = 28)	<i>P</i> Value
Male:female ratio	24:15	18:10	.2
Age (y)	60.5 ± 11.1 (39–77)	60.6 ± 9.7 (43–77)	.9
Age of male participants (y)	61.7 ± 11.9 (39–77)	60.6 ± 10.9 (43–77)	.8
Age of female participants (y)	58.7 ± 9.9 (39–73)	60.6 ± 7.4 (47–74)	.8
Site onset (limb:bulbar)	NA	18:10	
Disease duration (mo)	NA	18 ± 12 (4–64)	
ALSFRS-R score (out of 48)	NA	38.4 ± 6.0 (26–48)	
MoCA total score (out of 30)	NA	24.6 ± 3.2 (18–30)	
ECAS total score (out of 136)	NA	100 ± 15.4 (58–123)	
MMSE score (out of 30)	28.6 ± 0.9 (28–30)	NA	

Note.—Where appropriate, values are given as means ± standard deviations, with ranges in parentheses. ALS = amyotrophic lateral sclerosis, ALSFRS-R = ALS Functional Rating Scale Revised, ECAS = Edinburgh Cognitive and Behavioral ALS Screen, MMSE = Mini-Mental State Examination, MoCA = Montreal Cognitive Assessment, NA = not applicable.

Diffusion MRI data were acquired by using a twice-refocused single-shot echo-planar imaging pulse sequence with 81/12700 ms, a matrix of 128 × 128, 72 sections, a voxel size of 2 × 2 × 2 mm³, and a bandwidth of 1628 Hz/pixel. A sequence of 30 diffusion-weighted acquisitions (*b* = 1000 sec/mm²) with diffusion encoding along 30 noncollinear orientations (Siemens “MDDW” shell) and two interleaved reference acquisitions was repeated twice. Parallel imaging was enabled (three-fold acceleration), for a total imaging time of 14 minutes 11 seconds.

The image acquisition protocol was optimized by J.A. and J.K., physicists with 15 and 20 years of experience in MRI research, respectively.

Data Reconstruction and Postprocessing

Structural MRI.—The following standard methods for voxel-based morphometry, cortical thickness measurements, and subcortical volumetry were applied: SPM12b v6080 (<http://www.fil.ion.ucl.ac.uk/spm>), FreeSurfer v5.3.0 (<http://surfer.nmr.mgh.harvard.edu>), and FSL v5.0.9 processing tools (<https://fsl.fmrib.ox.ac.uk/fsl/fslwiki/FIRST>), respectively.

Susceptibility MRI.—Coil-specific data were combined by using a modified adaptive algorithm (13,14). Combined phase images were then “unwrapped” with a Laplacian approach (15), and the local field was revealed by means of spherical mean-value filtering (16) using a kernel radius of 5 mm. Susceptibility maps were then estimated by using the nonlinear morphology-enabled dipole inversion algorithm (17) with the regularization parameter set to an empirically optimized value of $\lambda = 1000$. To avoid assumptions about areas being spared in ALS, QSM values were not referenced. Susceptibility maps were spatially standardized with the aid of T1-weighted data by using a previously described ANTs v2.1.0 routine (<http://stnava.github.io/ANTs>) (14).

Diffusion MRI.—Diffusion-tensor imaging (DTI) was processed with standard FSL tools (<https://fsl.fmrib.ox.ac.uk/fsl/fslwiki/TBSS>), resulting in whole-brain skeletonized fractional

anisotropy and mean, radial, and axial diffusivity data for each participant.

Regional extractions.—Median QSM values were extracted bilaterally from major subcortical structures by applying the FSL-FIRST (FMRIB's Integrated Registration and Segmentation Tool) algorithm to our anatomic study template. QSM data were also extracted from previously validated manual segmentations of the red nucleus, substantia nigra (SN), and cerebellar dentate nucleus (14). Further segmentation of the SN was achieved through manual tracing of a (dorsal) T1-weighted hyperintense band highly colocalized with the anatomic site of the SN pars compacta. Finally, all subcortical regions of interest (ROIs) were eroded by convolution with a 1-mm-radius spherical kernel. Cortical ROIs for the motor cortex (precentral gyrus) and the pars opercularis of the inferior frontal gyrus were also examined; these were defined from a gyral-based digital atlas (<http://www.mindboggle.info/data.html>) by using a previously proposed approach (18). Median DTI parameter values were calculated for the corticospinal tract (CST) by intersection with a standard digital atlas (<http://cmrm.med.jhmi.edu>). Subsequently, median QSM values (across the same skeletonized CST mask) were also extracted in studywise space. All ROIs investigated are illustrated in Figure 2. Data processing was performed by J.A. and N.S. (an imaging researcher with 8 years of experience).

Statistical Analysis

Demographic analysis.—Sex and age differences between groups were assessed with a χ^2 test of independence and two-sample Wilcoxon rank-sum tests, respectively.

Structural MRI analysis.—Between-group statistical comparisons were performed with standard methods and a family-wise error (FWE)-adjusted statistical cutoff of $P < .05$. SPM corrects for FWE (both at voxel and cluster levels) by using random-field theory. FreeSurfer implements a cluster-wise Monte Carlo simulation procedure for FWE correction on surfaces.

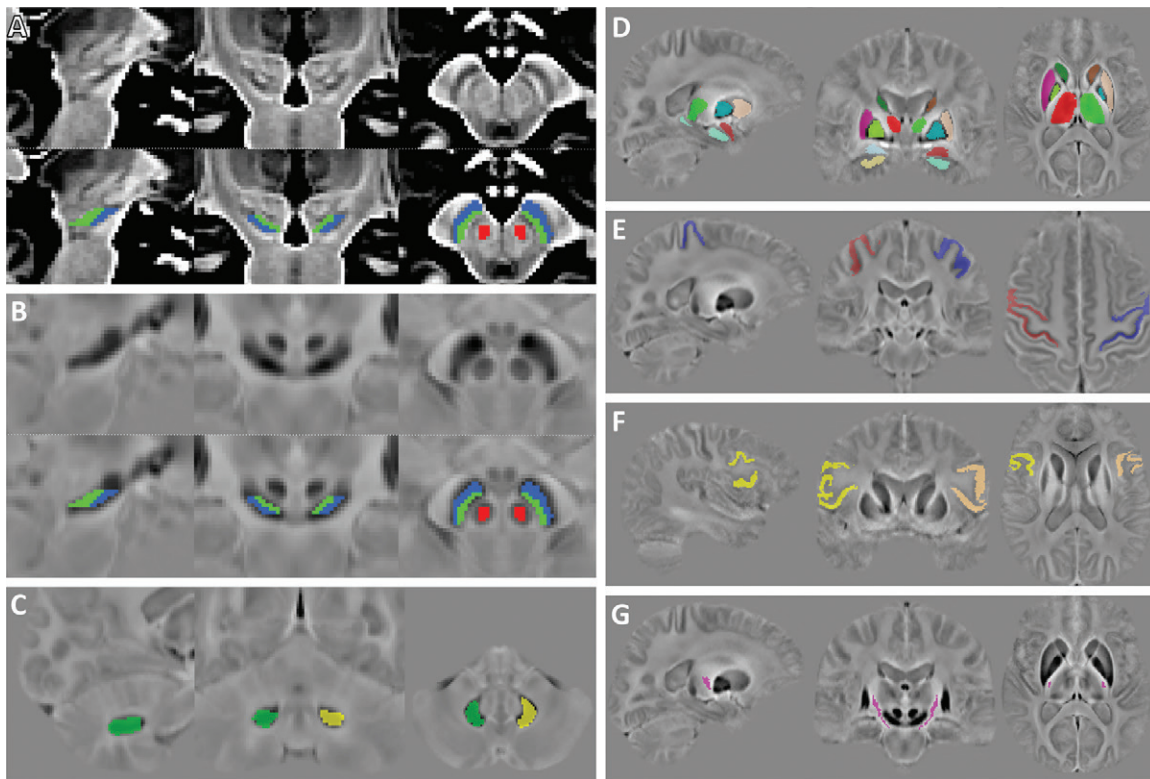


Figure 2: Images show selected regions of interest (ROIs) overlaid onto, *A*, T1-weighted and, *B–G*, quantitative susceptibility mapping study templates. *A, B*, Midbrain ROIs: dorsal/ventral substantia nigra subdivision and red nucleus. *C*, Cerebellar dentate nucleus. *D*, FIRST (FMRIB's Integrated Registration and Segmentation Tool) subcortical extractions. *E*, Precentral gyrus. *F*, Inferiofrontal pars opercularis. *G*, Corticospinal tract.

The Bonferroni procedure was used for FWE correction of deep gray matter volumetric measurements.

Whole-brain QSM analysis.—Absolute QSM data—used to prevent convolution-driven cancellations of spatially-adjacent positive/negative susceptibilities (19)—were smoothed (Gaussian kernel, standard deviation: 3 mm) and compensated for brain-boundary effects (19). On the assumption that age dispersion in our study (39–77 years old) could introduce spurious age-related QSM variance (14), the cross-sectional (ALS vs control) design included age as a nuisance covariate. Finally, whole-brain analysis was performed with threshold-free cluster-enhanced permutation statistics by using FSL tools (<http://fsl.fmrib.ox.ac.uk/fsl/fslwiki/Randomise>). Significant clusters were inferred from 20 000 data permutations and were reported at FWE $P < .05$. Subsequently after analysis, the QSM template and statistical maps were warped into MNI152 space (Montreal Neurologic Institute, McGill University, Canada) by using ANTs tools.

Regional QSM analysis.—Signed QSM data were regionally assessed to resolve the polarity of the QSM effects identified in the whole-brain study. In gray-matter ROIs, QSM distributions were not normally distributed; therefore, nonparametric statistics were used throughout. QSM laterality effects in patients with ALS were probed by using Wilcoxon signed-rank tests; these returned left/right differences ($P < .001$) for both SN subdivisions

and pars opercularis ROIs. For all other regions, QSM values were averaged across hemispheres. Subsequently, regional QSM values were age-corrected by using the covariance method (20), and cross-sectional QSM comparisons (ALS vs control subjects) were performed by using two-tailed Wilcoxon rank-sum tests. For ROIs returning cross-sectional alterations, Spearman rank correlation tests were then performed to explore a potential relationship between QSM and clinical severity scores.

CST correlation study.—Because past ALS studies have reported fractional anisotropy abnormalities along the CSTs (21,22), we investigated whether QSM might be sensitive to the same underlying mechanisms detected with DTI. Spearman rank-correlation tests were performed on the null hypothesis that QSM does not covary with DTI metrics in the ALS CST. All statistical analyses were performed by J.A.

Results

Structural measures—subcortical volumetry, voxel-based morphometry, and cortical thickness analysis—were all negative in age-corrected ALS-versus-control comparisons at FWE $P < .05$. The FWE-corrected absolute QSM results illustrated in Figure 3, however, revealed anatomically confluent alterations selectively in the motor cortex (Montreal Neurologic Institute $z = +26$ to $+68$ mm) extensively across most of the motor cortex but also including premotor medial areas and the primary somatosensory field; in the CST

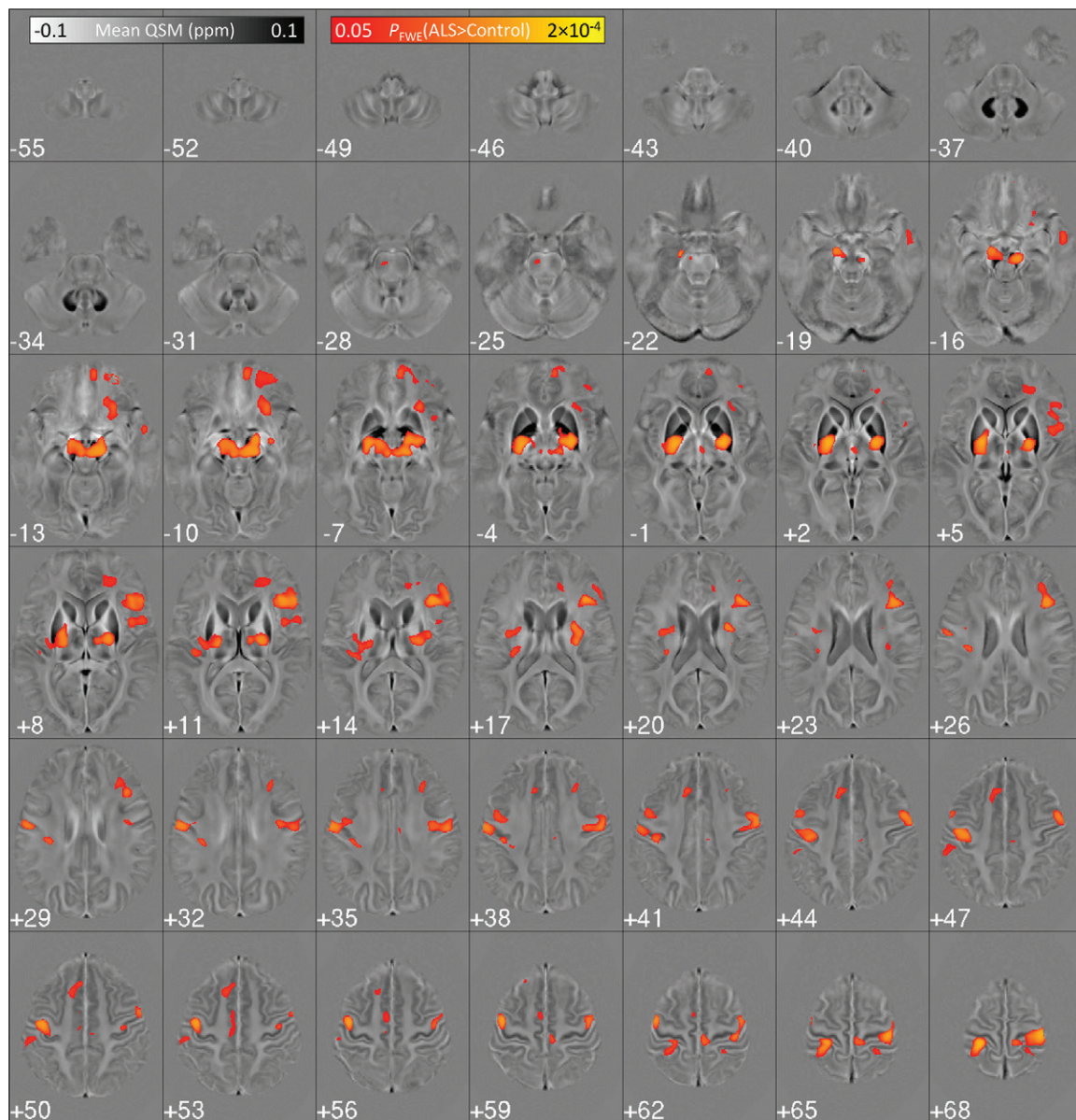


Figure 3: Cluster-enhanced quantitative susceptibility mapping (QSM) group statistics in 28 patients with amyotrophic lateral sclerosis (ALS) versus 39 elderly control subjects. Age-corrected absolute QSM was greater in patients than in control subjects. Red/yellow clusters = statistical differences at a family-wise error (FWE) P value of less than .05, which are overlaid onto the study-wise QSM template in the Montreal Neurologic Institute 152 coordinate system. High QSM appears as hypointensity (dark areas). (Although some past studies have opted to depict high QSM values as bright, the present scheme was chosen to be consistent with the susceptibility-weighted convention of depicting strong susceptibility weighting as dark.)

at the level of the posterior limb of the internal capsule ($z = -7$ to $+17$ mm); in the posterior corpus striatum ($z = -7$ to $+5$ mm), centered primarily on the globus pallidus (GP) but also including the posterior putamen; in the mesencephalon ($z = -16$ to -7 mm), including the SN and red nucleus; and in the prefrontal cortex ($z = -13$ to $+38$ mm), most prominently in the pars opercularis of the inferior frontal region but also (albeit more patchy and less intense) in the middle prefrontal, orbitofrontal frontal pole, and left anterior temporal lobe. In contrast, QSM group differences in parietal (excluding post-central gyrus), occipital, cerebellar, and medullopontine areas were statistically unremarkable. No lower absolute QSM

values in ALS were identified at FWE $P < .05$. In addition, exploratory limb-versus-bulbar whole-brain comparisons were also negative at FWE $P < .05$. All results remained unchanged (FWE $P < .05$) when gene-mutation carriers were excluded.

Our age-corrected regional study confirmed the selective pattern of QSM alterations in ALS (Fig 4). Our SN subdivision study revealed both dorsal (right: $Z = 3.0$, $P = .003$) and ventral (left: $Z = 3.3$, $P = .001$; right: $Z = 3.2$, $P = .001$) involvement in the form of higher signed QSM values in the ALS group, although with a ventral bias because of the relatively normal profile observed for the left dorsal SN ($Z = 1.4$, $P = .18$). Signed QSM in the motor cortex ($Z = 3.3$, $P < .001$) and GP ($Z = 3.0$,

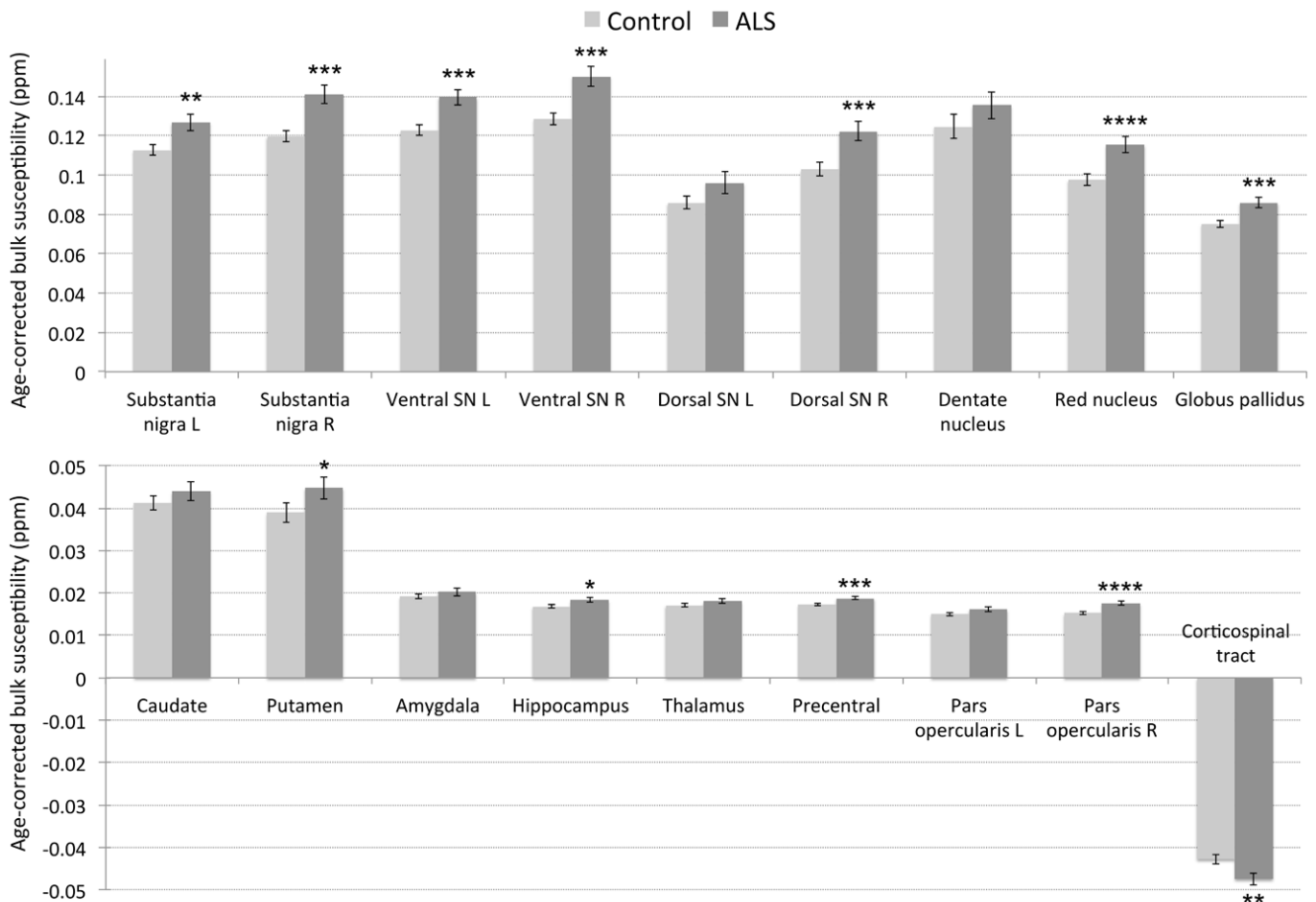


Figure 4: Bar graph shows age-adjusted signed quantitative susceptibility mapping group statistics. Summary statistics are means \pm standard errors of the mean. Asterisks = the strength of the group difference—that is, * = $P < .05$; ** = $P < .01$; *** = Bonferroni-corrected $P < .05$; and **** = Bonferroni-corrected $P < .01$. ALS = amyotrophic lateral sclerosis, L = left, ppm = parts per million, R = right, SN = substantia nigra.

$P = .003$) and particularly in the red nucleus ($Z = 3.6, P < .001$) and right pars opercularis ($Z = 3.9, P < .001$) were also higher in patients with ALS. More subtle effects, however, were observed in the putamen ($Z = 2.0, P = .04$) and hippocampus ($Z = 2.1, P = .04$), while a reversed pattern (lower QSM in ALS) was found in the CST ($Z = -2.6, P = .01$). In contrast, the dentate nucleus ($Z = 1.6, P = .1$), the caudate nucleus ($Z = 0.7, P = .5$), the amygdala ($Z = 0.8, P = .4$), and the left pars opercularis ($Z = 1.7, P = .09$) remained relatively unchanged.

Magnified views of affected structures demonstrated QSM abnormalities that were apparent at visual inspection in most individual patients in contrast to matched control subjects (Fig 5). Visual inspection of the data also suggested that QSM for the SN and GP appeared to be covarying with each other in ALS. Formal investigation of this observation by using a Spearman rank-correlation test indeed confirmed that age-corrected SN and GP QSM values were moderately correlated ($\rho^2 = 0.42, P < .001$) in ALS, whereas no such correlation was evident in control subjects ($\rho^2 = 0.07, P = .1$).

We subsequently investigated whether such a relationship held true for disease-onset type and sex-specific patient subgroups on the basis that age-adjusted QSM values were greater in GP and SN ROIs for bulbar-onset ALS (QSM = 0.095 ppm

± 0.012 in GP; QSM = 0.148 ppm ± 0.021 in SN) than for limb-onset ALS (QSM = 0.084 ppm ± 0.014 in GP; QSM = 0.130 ppm ± 0.019 in SN) and, in the GP only, for female patients (QSM = 0.095 ppm ± 0.014) versus male patients (QSM = 0.081 ppm ± 0.014). Sex effects were absent in control subjects for any ROI ($P > .1$). Such exploratory investigations revealed SN and GP QSM associations for all subgroups (limb: $\rho^2 = 0.26, P = .03$; bulbar: $\rho^2 = 0.81, P = .001$; male: $\rho^2 = 0.50, P = .001$; female: $\rho^2 = 0.45, P = .02$).

Post-hoc Spearman correlation tests investigating the covariance between age-adjusted QSM values and ALS clinical scores (controlling for disease-onset type and sex differences in the SN and GP) were all negative (SN: $\rho^2_{ALSFRS-R} = 0.06, P = .3, \rho^2_{ECAS} = 0.11, P = .1$; GP: $\rho^2_{ALSFRS-R} = 0.01, P = .7, \rho^2_{ECAS} = 0.04, P = .4$; red nucleus: $\rho^2_{ALSFRS-R} = 0.01, P = .8, \rho^2_{ECAS} = 0.05, P = .3$; motor cortex: $\rho^2_{ALSFRS-R} = 0.01, P = .9, \rho^2_{ECAS} = 0.09, P = .1$; CST: $\rho^2_{ALSFRS-R} = 0.03, P = .5, \rho^2_{ECAS} = 0.01, P = .6$; and left pars opercularis: $\rho^2_{ALSFRS-R} = 0.01, P = .8, \rho^2_{ECAS} = 0.03, P = .4$).

Given the unexpected behavior of lower QSM in the ALS CST, a further correlation analysis was performed to test whether this effect could be driven by QSM-inversion residuals emanating from the adjacent GP; the result was negative ($\rho^2 = 0.05, P = .3$).

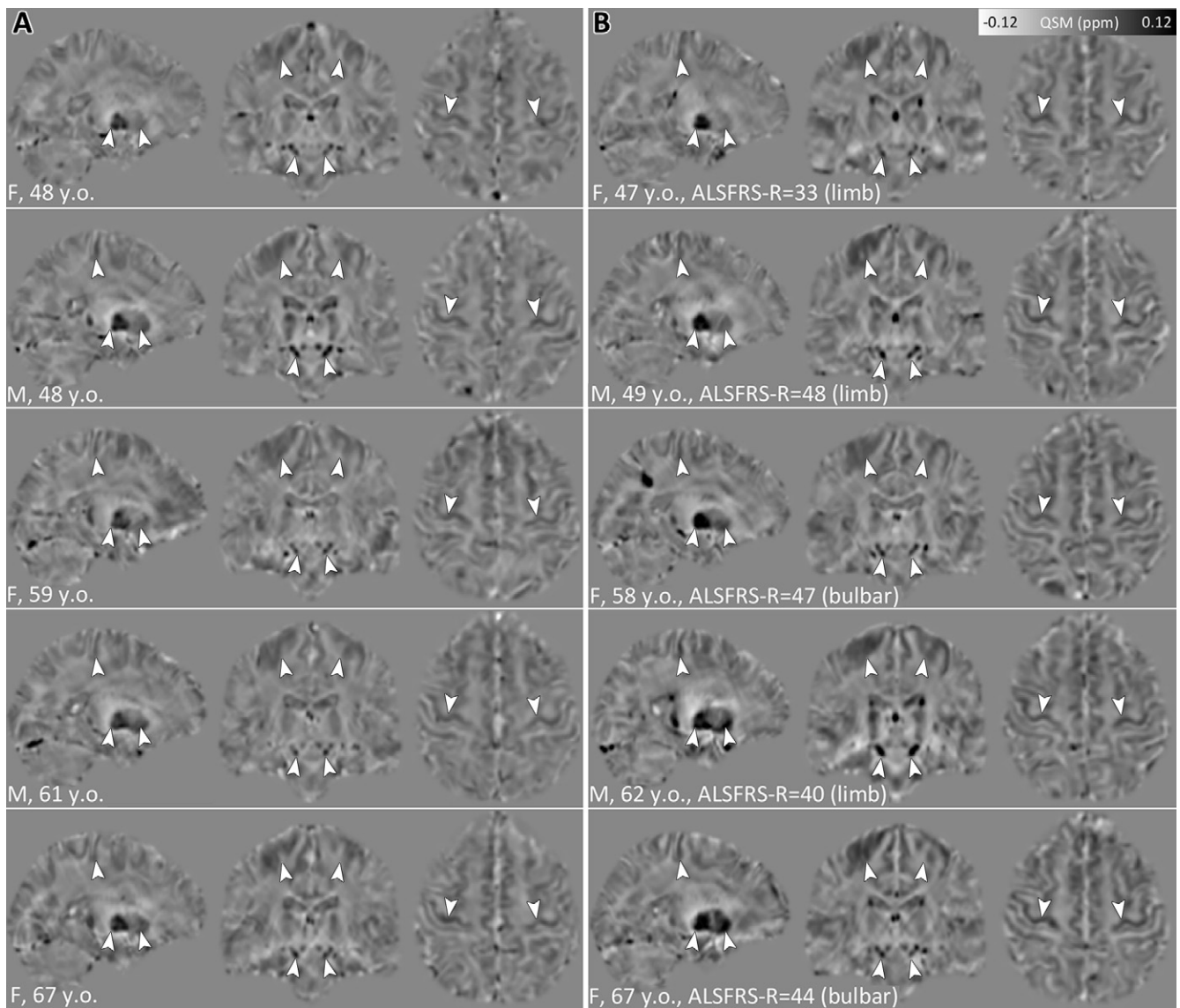


Figure 5: Representative sagittal, coronal, and axial quantitative susceptibility mapping (QSM) views in standard space in, *A*, five control subjects and, *B*, five age-matched patients with amyotrophic lateral sclerosis (ALS). Arrowheads = some regions of QSM increase in ALS: precentral gyrus (all views), corpus striatum (sagittal view), and mesencephalon (coronal view). ALSFRS-R = ALS Functional Rating Scale Revised, F = female, M = male, y.o. = years old.

Finally, our correlation study investigating the covariance of QSM and DTI metrics in the CST revealed a positive effect for QSM and fractional anisotropy ($\rho^2 = 0.25$, $P = .007$) and a negative effect for QSM and radial diffusivity ($\rho^2 = 0.25$, $P = .007$) and QSM and mean diffusivity ($\rho^2 = 0.25$, $P = .007$), while the QSM and axial diffusivity correlation was not significant ($\rho^2 = 0.01$, $P = .7$).

Discussion

This study identified evidence for increased tissue iron loading in ALS in several brain regions, most notably the motor cortex, SN, GP, red nucleus, and putamen. The increased iron concentration in the SN and GP appeared to be occurring in concert in that the values for these regions were correlated in the ALS group. Lower magnetic susceptibility, meanwhile, was identified

in the CST; the magnitude of this decrease was correlated with DTI metrics such as fractional anisotropy in this tract.

QSM increase indicative of increased iron concentration in the primary motor cortex was an expected result in light of post-mortem reports of Betz cell loss (23), intraneuronal TDP-43 immunoreactivity (3) and, most notably, ferritin-positive microglia and macrophages (24,25). Such studies suggest primarily that motor cortex neuronal and glial pTDP-43 inclusions are one of the earliest pathologic events in ALS and colocalize with iron-laden reactive microglia. Several MRI parameters have captured abnormalities in the motor cortex of ALS, namely, fluid-attenuated inversion recovery imaging (8,25), apparent transverse relaxation time ($T2^*$) (25,26), and, more recently, susceptibility-weighted imaging (24). In ROI studies, MR measurements such as QSM (8,26) and MR spectroscopy (27)

have further characterized these effects, with indications that QSM might be a sensitive marker of motor cortex pathology in ALS (8). Our results extend these findings in demonstrating that QSM abnormalities in the motor cortex of ALS are now detectable with an unbiased whole-brain method. Meanwhile, PET imaging studies have demonstrated microglial activation in ALS, with one of the principal loci being the motor cortex (28). Increased QSM values in patients with ALS compared with control subjects consistent with iron accumulation suggest a proactive role for metals in oxidative stress–induced cell death and, possibly, pTDP-43 accumulation (4); excess iron found in microglia might be due to phagocytosis of degenerating iron-containing neurons and glial cells (25).

Cortical QSM increases in patients with ALS compared with control subjects beyond the primary motor area were almost exclusively restricted to frontal regions, with the largest cluster extensively involving the inferior frontal cortex but spreading across several other frontal areas. These results are concordant with other ALS imaging findings in showing that extramotor involvement, when present, has a characteristic frontal predilection for cortical atrophy (29), white matter disruption (22), glucose hypometabolism (30), and microglial activation (28).

Axonal efferents from the motor cortex pass into the CST. Previous longitudinal DTI work in ALS demonstrated that degeneration in the CST, as measured by decline in fractional anisotropy, is essentially linear and, furthermore, is more sensitive to change than motor cortex atrophy (31). It appears that QSM is also sensitive to CST degeneration. Our study found that QSM values in ALS were correlated with DTI parameters in this tract. Interestingly, however, susceptibility values in the ALS CST were in the opposite direction from those observed for gray-matter structures. That is, more negative than in control subjects, indicating a shift toward greater diamagnetism, the magnitude of which was correlated with DTI metrics. The mechanism underlying this diamagnetic shift is unclear. It is unlikely iron accumulation or demyelination could have driven this effect; however, these cannot be ruled out because the exact contributions driving susceptibility polarity in white matter are still unclear because of inconsistencies between theoretical models and empirical data (32). However, the correlations with diffusion metrics argue strongly against this being a spurious finding and suggest that changes in the CST with QSM in some way reflect altered tissue microstructure (33).

Beyond the pyramidal system, several subcortical structures relevant to motor function showed higher QSM in ALS, namely, the SN, GP, putamen, and red nucleus. Subclinical involvement of the nigrostriatal pathway has also been previously demonstrated by using 6-fluorodopa PET (34), while the red nucleus is one first sites of pTDP-43 pathology after the primary motor nuclei (3). Interestingly, a volumetric study (29) focusing on subcortical structures found significant group-level atrophy in several striatal nuclei for patients with advanced ALS with comorbid behavioral variant FTD but not in patients with mild or no cognitive impairment. The results of our deep-brain volumetry study in ALS without dementia were also negative, standing in stark contrast to

the QSM results. This observation suggests that QSM, overall, is more sensitive than conventional structural MRI for detecting abnormalities in ALS and could also be an indication that QSM might be revealing an upstream event of cell loss.

Furthermore, the correlation between nigral and pallidal QSM in ALS suggests that these two structures are affected in concert by iron accumulation. Finally, there was a weak effect in the hippocampus, in keeping with structural imaging findings in this region in ALS (29); the effect size, however, was very small, particularly considering that hippocampal QSM values are very small in the control population.

Our study had some limitations. First, QSM values were not normalized to a reference region, which might have introduced spurious variability. Second, we were unable to establish QSM correlates of clinical severity measures. However, given the narrow spread of severity scores for our patient cohort and a relatively low number of subjects for regression analyses, the risk of false-negative associations was very high. This is an important caveat of our study. Further studies with greater statistical power and greater spread of clinical severity scores (as well as complete genetic profiling) will be required to definitively address this issue. Our results might have also benefited from controlling for potential disease-onset type and sex in the patient population. A final limitation is that there was no postmortem measurement of regional brain iron concentration in the study population to confirm that this was definitely the cause of increased QSM values; however, the known regional variations in brain iron concentration from postmortem measurements agree very closely with that previously seen using the QSM method (14).

In conclusion, increased QSM values consistent with iron accumulation in ALS involved the motor cortex and a range of subcortical nuclei. This distribution is consistent with the known pattern of degeneration. Interestingly, qualitatively different QSM patterns are emerging in the major neurodegenerative diseases—eg, ALS in the present study, Parkinson disease (18), and Alzheimer disease (35)—that might offer insights for pathologic mechanisms beyond the standard distribution of histopathologic inclusions.

Author contributions: Guarantors of integrity of entire study, J.A., S.A., S.V., P.J.N.; study concepts/study design or data acquisition or data analysis/interpretation, all authors; manuscript drafting or manuscript revision for important intellectual content, all authors; manuscript final version approval, all authors; agrees to ensure any questions related to the work are appropriately resolved, all authors; literature research, J.A., J.M., S.A., K.K., S.P., N.S., J.K., R.D., S.V., P.J.N.; clinical studies, J.A., S.S., S.A., K.K., S.P., N.S., J.K., S.V., P.J.N.; experimental studies, J.A., J.M., H.J.H., S.V., P.J.N.; statistical analysis, J.A., P.J.N.; and manuscript editing, J.A., J.M., S.A., K.K., S.P., N.S., J.K., H.J.H., R.D., S.V., P.J.N.

Disclosures of Conflicts of Interest: J.A. disclosed no relevant relationships. J.M. disclosed no relevant relationships. S.S. disclosed no relevant relationships. S.A. disclosed no relevant relationships. K.K. disclosed no relevant relationships. S.P. Activities related to the present article: disclosed no relevant relationships. Activities not related to the present article: institution has grants or grants pending from the German Neuromuscular Society, Federal Ministry of Education and Research and the Petermax-Müller Foundation; is on the speakers bureau of Desitin Arzneimittel, Cytokinetics, and TEVA Pharmaceuticals; has received travel funds from Biogen, Glaxo Smith Kline, Cytokinetics, and Orion Pharma; institution has received financial support for the conduct of clinical trials from Biogen, Glaxo Smith Kline, Cytokinetics, and Orion Pharma. Other relationships: disclosed no relevant relationships. N.S. disclosed no relevant relationships. J.K. disclosed no relevant relationships. H.J.H. disclosed no relevant relationships. R.D. Activities re-

lated to the present article: disclosed no relevant relationships. Activities not related to the present article: has received royalties from Thieme Publishing House. Other relationships: disclosed no relevant relationships. **S.V.** disclosed no relevant relationships. **P.J.N.** disclosed no relevant relationships.

References

- Lomen-Hoerth C, Murphy J, Langmore S, Kramer JH, Olney RK, Miller B. Are amyotrophic lateral sclerosis patients cognitively normal? *Neurology* 2003;60(7):1094–1097.
- Neumann M, Sampathu DM, Kwong LK, et al. Ubiquitinated TDP-43 in frontotemporal lobar degeneration and amyotrophic lateral sclerosis. *Science* 2006;314(5796):130–133.
- Brettschneider J, Del Tredici K, Toledo JB, et al. Stages of pTDP-43 pathology in amyotrophic lateral sclerosis. *Ann Neurol* 2013;74(1):20–38.
- Lovejoy DB, Guillemin GJ. The potential for transition metal-mediated neurodegeneration in amyotrophic lateral sclerosis. *Front Aging Neurosci* 2014;6:173.
- Wang Q, Zhang X, Chen S, et al. Prevention of motor neuron degeneration by novel iron chelators in SOD1(G93A) transgenic mice of amyotrophic lateral sclerosis. *Neurodegener Dis* 2011;8(5):310–321.
- Jeong SY, Rathore KI, Schulz K, Ponka P, Arosio P, David S. Dysregulation of iron homeostasis in the CNS contributes to disease progression in a mouse model of amyotrophic lateral sclerosis. *J Neurosci* 2009;29(3):610–619.
- Wang Y, Liu T. Quantitative susceptibility mapping (QSM): decoding MRI data for a tissue magnetic biomarker. *Magn Reson Med* 2015;73(1):82–101.
- Schweitzer AD, Liu T, Gupta A, et al. Quantitative susceptibility mapping of the motor cortex in amyotrophic lateral sclerosis and primary lateral sclerosis. *AJR Am J Roentgenol* 2015;204(5):1086–1092.
- Chiò A, Calvo A, Moglia C, Mazzini L, Mora G; PARALS study group. Phenotypic heterogeneity of amyotrophic lateral sclerosis: a population based study. *J Neurol Neurosurg Psychiatry* 2011;82(7):740–746.
- Schreiber S, Abdulla S, Debska-Vielhaber G, et al. Peripheral nerve ultrasound in amyotrophic lateral sclerosis phenotypes. *Muscle Nerve* 2015;51(5):669–675.
- Brooks BR, Miller RG, Swash M, Munsat TL; World Federation of Neurology Research Group on Motor Neuron Diseases. El Escorial revisited: revised criteria for the diagnosis of amyotrophic lateral sclerosis. *Amyotroph Lateral Scler Other Motor Neuron Disord* 2000;1(5):293–299.
- Rascovsky K, Hodges JR, Knopman D, et al. Sensitivity of revised diagnostic criteria for the behavioural variant of frontotemporal dementia. *Brain* 2011;134(Pt 9):2456–2477.
- Walsh DO, Gmitro AF, Marcellin MW. Adaptive reconstruction of phased array MR imagery. *Magn Reson Med* 2000;43(5):682–690.
- Acosta-Cabronero J, Betts MJ, Cardenas-Blanco A, Yang S, Nestor PJ. In vivo MRI mapping of brain iron deposition across the adult lifespan. *J Neurosci* 2016;36(2):364–374.
- Schofield MA, Zhu Y. Fast phase unwrapping algorithm for interferometric applications. *Opt Lett* 2003;28(14):1194–1196.
- Schweser F, Deistung A, Lehr BW, Reichenbach JR. Quantitative imaging of intrinsic magnetic tissue properties using MRI signal phase: an approach to in vivo brain iron metabolism? *Neuroimage* 2011;54(4):2789–2807.
- Liu T, Wisnieff C, Lou M, Chen W, Spincemaille P, Wang Y. Nonlinear formulation of the magnetic field to source relationship for robust quantitative susceptibility mapping. *Magn Reson Med* 2013;69(2):467–476.
- Acosta-Cabronero J, Cardenas-Blanco A, Betts MJ, et al. The whole-brain pattern of magnetic susceptibility perturbations in Parkinson's disease. *Brain* 2017;140(1):118–131.
- Betts MJ, Acosta-Cabronero J, Cardenas-Blanco A, Nestor PJ, Düzel E. High-resolution characterisation of the aging brain using simultaneous quantitative susceptibility mapping (QSM) and R2* measurements at 7T. *Neuroimage* 2016;138:43–63.
- Jack CR Jr, Twomey CK, Zinsmeister AR, Sharbrough FW, Petersen RC, Cascino GD. Anterior temporal lobes and hippocampal formations: normative volumetric measurements from MR images in young adults. *Radiology* 1989;172(2):549–554.
- Cardenas-Blanco A, Machts J, Acosta-Cabronero J, et al. Central white matter degeneration in bulbar- and limb-onset amyotrophic lateral sclerosis. *J Neurol* 2014;261(10):1961–1967.
- Kasper E, Schuster C, Machts J, et al. Microstructural white matter changes underlying cognitive and behavioural impairment in ALS—an in vivo study using DTI. *PLoS One* 2014;9(12):e114543.
- Udaka F, Kameyama M, Tomonaga M. Degeneration of Betz cells in motor neuron disease. A Golgi study. *Acta Neuropathol (Berl)* 1986;70(3-4):289–295.
- Adachi Y, Sato N, Saito Y, et al. Usefulness of SWI for the detection of iron in the motor cortex in amyotrophic lateral sclerosis. *J Neuroimaging* 2015;25(3):443–451.
- Kwan JY, Jeong SY, Van Gelderen P, et al. Iron accumulation in deep cortical layers accounts for MRI signal abnormalities in ALS: correlating 7 tesla MRI and pathology. *PLoS One* 2012;7(4):e35241.
- Costagli M, Donatelli G, Biagi L, et al. Magnetic susceptibility in the deep layers of the primary motor cortex in amyotrophic lateral sclerosis. *Neuroimage Clin* 2016;12:965–969.
- Pyra T, Hui B, Hanstock C, et al. Combined structural and neurochemical evaluation of the corticospinal tract in amyotrophic lateral sclerosis. *Amyotroph Lateral Scler* 2010;11(1-2):157–165.
- Turner MR, Cagnin A, Turkheimer FE, et al. Evidence of widespread cerebral microglial activation in amyotrophic lateral sclerosis: an [11C](R)-PK11195 positron emission tomography study. *Neurobiol Dis* 2004;15(3):601–609.
- Machts J, Loewe K, Kaufmann J, et al. Basal ganglia pathology in ALS is associated with neuropsychological deficits. *Neurology* 2015;85(15):1301–1309.
- Quartuccio N, Van Weehaeghe D, Cistaro A, Jonsson C, Van Laere K, Pagani M. Positron emission tomography neuroimaging in amyotrophic lateral sclerosis: what is new? *Q J Nucl Med Mol Imaging* 2014;58(4):344–354.
- Cardenas-Blanco A, Machts J, Acosta-Cabronero J, et al. Structural and diffusion imaging versus clinical assessment to monitor amyotrophic lateral sclerosis. *Neuroimage Clin* 2016;11:408–414.
- Duyn JH. Frequency shifts in the myelin water compartment. *Magn Reson Med* 2014;71(6):1953–1955.
- Wharton S, Bowtell R. Effects of white matter microstructure on phase and susceptibility maps. *Magn Reson Med* 2015;73(3):1258–1269.
- Takahashi H, Snow BJ, Bhatt MH, Peppard R, Eisen A, Calne DB. Evidence for a dopaminergic deficit in sporadic amyotrophic lateral sclerosis on positron emission scanning. *Lancet* 1993;342(8878):1016–1018.
- Acosta-Cabronero J, Williams GB, Cardenas-Blanco A, Arnold RJ, Lupson V, Nestor PJ. In vivo quantitative susceptibility mapping (QSM) in Alzheimer's disease. *PLoS One* 2013;8(11):e81093.